Vol. 26 • No. 33 • September 6 • 2016

www.afm-journal.de

ADVANCED FUNCTIONAL MATERIALS

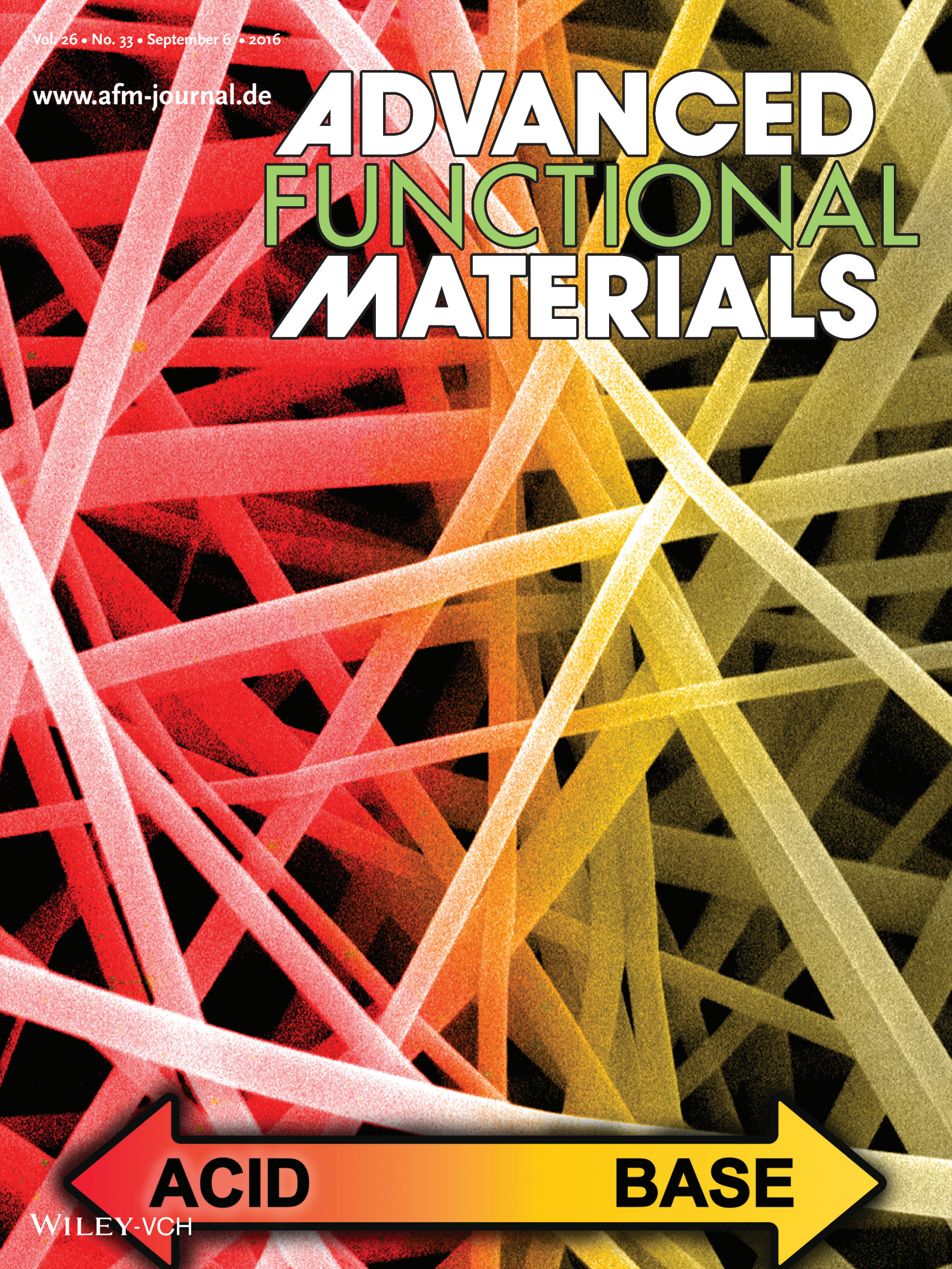

WILEY-VCH

ADVANCED FUNCTIONAL MATERIALS
www.afm-journal.de

Dye Modification of Nanofibrous Silicon Oxide Membranes for Colorimetric HCl and NH_3 Sensing

Jozefien Geltmeyer, Gertjan Vancoillie, Iline Steyaert, Bet Breyne, Gabriella Cousins, Kathleen Lava, Richard Hoogenboom, Klaartje De Buysser,* and Karen De Clerck**

Colorimetric sensors for monitoring and visual reporting of acidic environments both in water and air are highly valuable in various fields, such as safety and technical textiles. Until now sol-gel-based colorimetric sensors are usually nonflexible bulk glass or thin-film sensors. Large-area, flexible sensors usable in strong acidic environments are not available. Therefore, in this study organically modified silicon oxide nanofibrous membranes are produced by combining electrospinning and sol-gel technology. Two pH-indicator dyes are immobilized in the nanofibrous membranes: methyl yellow via doping, methyl red via both doping, and covalent bonding. This resulted in sensor materials with a fast response time and high sensitivity for pH-change in water. The covalent bond between dye and the sol-gel network showed to be essential to obtain a reusable pH-sensor in aqueous environment. Also a high sensitivity is obtained for sensing of HCl and NH_3 vapors, including a memory function allowing visual read-out up to 20 min after exposure. These fast and reversible, large-area flexible nanofibrous colorimetric sensors are highly interesting for use in multiple applications such as protective clothing and equipment. Moreover, the sensitivity to biogenic amines is demonstrated, offering potential for control and monitoring of food quality.

1. Introduction

Colorimetric sensor materials are of great interest in various fields such as environmental control, safety, industrial plants, etc. Ceramic sol-gel based sensors are highly valuable due to their high chemical and temperature resistance. The majority of the studied sol-gel sensors are sensors for pH-measurements.[1–5] These pH-sensors are usually optical bulk glass or thin films.[4,6–9] pH-sensors are not only developed to detect acidity changes in aqueous solutions, the detection of HCl and NH_3 gas has also recently attracted significant attention.[10–13] The detection of these gases via optical sensors in industrial processes are of great interest, due to their simplicity and sensitivity. To obtain a flexible and large-area sensor, the combination of sol-gel and textiles can be highly valuable. Coating on textiles via sol-gel has shown to be very promising to produce pH-sensitive textiles.[14] Combining sol-gel and textiles can result in sensor materials with highly promising characteristics. Such lightweight materials have a high flexibility, reusability, breathability, and mechanical stability. Moreover, these halochromic textiles can cover a large surface but still result in a local signal. They can be of great interest in various fields such as filtration, safety, and technical textiles.[15]

Improvement of the sensitivity of colorimetric textile sensors is needed and can be carried out by diminishing the fiber diameters.[16,17] Nanofibrous membranes, obtained via the electrospinning process, are known for their unique properties due to their small fiber diameters.[18–23] These membranes have a small pore size, high porosity, and large surface area. These unique properties offer potentials for an improved sensor sensitivity and response time, highly desired for sensor applications. Halochromic polymer nanofibers have been successfully produced.[15–17,24,25] Upscaling of the process resulted in large-area sensors. A disadvantage of these polymer nanofibers is however their low temperature resistance and their low resistance to strong acidic and/or basic environments making them less suitable in pH-sensor applications under harsh conditions. For these harsh environments ceramic nanofibers would be highly valuable. Moreover, the sol-gel process offers various possibilities for functionalization through the selection of an

J. Geltmeyer, Dr. I. Steyaert, B. Breyne, G. Cousins, Prof. K. De Clerck
Fibre and Colouration Technology Research Group
Department of Textiles
Faculty of Engineering and Architecture
Ghent University
Technologiepark 907, 9052 Ghent, Belgium
E-mail: Karen.DeClerck@UGent.be

Dr. G. Vancoillie, Dr. K. Lava, Prof. R. Hoogenboom
Supramolecular Chemistry Group
Department of Organic and Macromolecular Chemistry
Faculty of Sciences
Ghent University
Krijgslaan 281 S4, 9000 Ghent, Belgium
E-mail: Richard.Hoogenboom@UGent.be

Prof. K. De Buysser
Sol-gel Centre for Research on Inorganic Powders and Thin Films Synthesis
Department of Inorganic and Physical Chemistry
Faculty of Sciences
Ghent University
Krijgslaan 281 S3, 9000 Ghent, Belgium
E-mail: Klaartje.DeBuysser@UGent.be

DOI: 10.1002/adfm.201602351

appropriate precursor. Incorporation of the pH-indicators in the sol-gel matrix can be carried out via doping or covalent bonding to the selected precursor. The addition of low molar mass components or nanoparticles to the electrospinning solution prior to fiber formation, i.e., doping, is the most frequently used strategy for nanofiber functionalization.[17,26–31] However, extended research on immobilization of pH-indicator dyes has shown that a covalent linkage between dye and matrix is the most efficient manner to inhibit dye migration.[2,32–36] To our knowledge, ceramic nanofibers that show a pH-sensing functionality have not been reported yet.

The combination of electrospinning and sol-gel has gained a lot of interest in recent years.[37–41] Most frequently, organic polymers are added to the alkoxide precursors to enable electrospinning, after which the polymer components are removed via a thermal treatment (typically above 400 °C).[42,43] We have recently shown that control of the viscosity, the condensation degree and amount of solvent allows for stable electrospinning of sols without the need for an additional organic polymer.[44,45] The electrospinning of pure tetraethylorthosilicate (TEOS) sols has been optimized to obtain uniform, beadless, large nanofibrous membranes. Although being more challenging, this is the preferred method to produce silicon oxide nanofibrous membranes for sensing applications. It makes the high temperature thermal treatment redundant, which would be deleterious not only for the nanofibrous structure but also for the introduced sensing functionality.

The aim of this research is to develop colorimetric nanofibrous sensors that can be used for both pH-sensing in aqueous solution as well as hydrogen chloride and ammonia vapor sensing. This shows potentials for multiple applications such as environmental control, industrial plants, protective clothing and equipment. To our knowledge silicon oxide-based, large-area flexible nanofibrous colorimetric sensors have not been reported before. In this study (3-aminopropyl)triethoxysilane (APTES) is selected as the additional precursor for functionalization. Thus, the electrospinning of TEOS-APTES sols needs to be tackled. The pH-indicator dyes methyl yellow (MY) and methyl red (MR) are added to these sols via dye doping. Additionally, the carboxylic acid group of methyl red offers the possibility for covalent linking to the APTES precursor and thus covalent immobilization in the silicon oxide nanofibers. These different types of nanofibrous membranes will be evaluated both for pH-sensing in water and for sensing of hydrogen chloride and ammonia vapors. To evaluate the versatility of the membranes also their sensitivity to biogenic amines was screened. Colorimetric sensors with a clear color change in response to changing acidity or alkalinity of water or air are aimed for. Flexible, large scale, reusable sensors which can be highly valuable for personal protective equipment are envisioned.

2. Results and Discussion

2.1. Functionalization of APTES with Methyl Red

The first goal in this paper is to modify the silica-precursor APTES with a suitable, pH-responsive dye to enable covalent immobilization of the chosen dye onto the fabricated, silica-based halochromic material. APTES was chosen as its amino group can easily be modified through carbodiimide-assisted amide coupling with the carboxylic acid group present in MR.[46] Similar MR was selected as dye because of the straightforward modification of its carboxylic acid group as well as its interesting pH-responsive color change for sensing of strong acid vapors. Various methods for the amide formation were investigated involving different coupling reagents including 1-ethyl-3-(3-dimethylaminopropyl)carbodiimide (EDC), *N,N′*-dicyclohexylcarbodiimide (DCC), and *N,N′*-diisopropylcarbodiimide (DIC) or a preceding activation step of MR as activated ester with *N*-hydroxysuccinimide (NHS) or pentafluorophenol (PFP) in an attempt to simplify the purification. Eventually, the modification was optimized to a simple one-step DCC-assisted coupling at room temperature and purification using a short silica column (eluent: EtOAc/n-Hexane 1/1). By adding APTES in excess, the MR-APTES could easily be isolated after complete consumption of MR since the residual APTES and formed dicyclohexylurea are completely retained on the column. After evaporation of the solvent, a dark red solid was obtained. The disadvantage of using a silica-based column for the purification of a silica precursor is the significant immobilization of MR-APTES on the column material, reducing the yield to 36%. The simple DCC-assisted coupling and the straightforward purification, however, does allow for the synthesis of large batches (>1 g MR-APTES).

2.2. Halochromic Behavior of MY, MR, and MR-APTES Aqueous Solutions

The functionalization of APTES with MR may have an influence on the color and color transitions of the dye, as the free carboxylic acid group is modified into an amide moiety. Therefore, it is essential to study and compare the behavior of the dyes MY, MR, and MR-APTES in solution. MR and MY have been profoundly studied in literature.[47–49] An overview of the changes in the molecular and electronic structure, responsible for the color changes on protonation are visualized in **Figure 1**. When APTES is coupled to MR, a covalent amide bond is formed between the carboxylic acid group of MR and the amine group of APTES removing the acidic proton of MR. As a consequence, the carboxylic acid group of the dye is no longer available to take part in the structural changes for the color transitions and it may be anticipated that the halochromic behavior of MR-APTES will be similar to that of MY (Figure 1b). Visible spectra of the three solutions (380–780 nm) were recorded at pH values from pH 1 to pH 12. The normalized absorbance spectra at pH 2 and pH 12 are shown in **Figure 2**a. The alkaline form of the dyes MR, MR-APTES, and MY with λ_{max} of 432, 451, and 446 nm, respectively, is responsible for the yellow color. Upon acidification all solutions change color from yellow over orange to red. MR has two red forms, one form associated with the monoprotonated form and the second with the diprotonated form, at pH 2 the λ_{max} of 519 nm can be attributed to the diprotonated form.[48] For MY and MR-APTES, on the contrary, the red color can be attributed to the monoprotonated form of the dye, having a λ_{max} of respectively 514 and

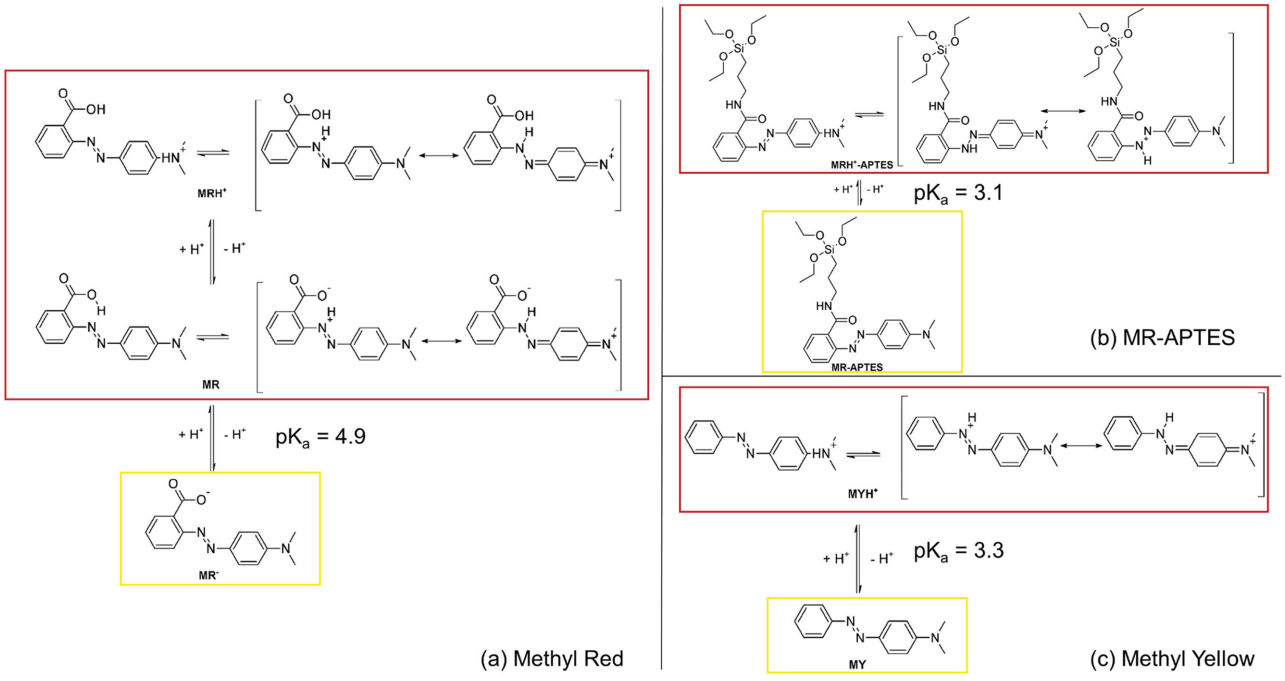

Figure 1. The acid–base equilibria of the dyes (a) methyl red, (b) MR-APTES, and (c) methyl yellow. The color of the frames visualizes the color of the dyes in their alkaline and protonated forms.

517 nm. A shift in pK_a is seen from 4.9 ± 0.2 for the MR solution to 3.1 ± 0.1 for the MR-APTES solution (Figure 2b), being similar to the pK_a of MY in solution 3.3 ± 0.01 (Figure 2c). In conclusion, the blocking of the acidic proton of MR as a result of APTES functionalization, results in a shift of the pK_a making the halochromic behavior of MR-APTES similar to MY. All three dyes showed a clear color shift in response to pH-changes, making them suitable for preparation of colorimetric sensors. The absence of the carboxylic group on the dye MY, however, makes it not suitable for covalent immobilization onto the silicon oxide nanofibers.

2.3. Electrospinning of Dye Functionalized Nanofibers

To produce colorimetric nanofibrous membranes, MY, MR, and MR-APTES were added to the sols prior to electrospinning. To electrospin TEOS-APTES sols with the aim for functionalized nanofibers, a sufficient amount of APTES needs to be selected that however still allows for a stable electrospinning process. Too high amounts of APTES, molar ratios of TEOS:APTES > 1:0.005, resulted in sols for which the viscosity increased too fast and gelation occurred too quick. A molar ratio of TEOS:APTES 1:0.0024 was found to correspond to a sufficient color depth of the final nanofibrous membranes as well as a good electrospinnability.

MY was added to TEOS/APTES (TA) sols, MR was added to both TEOS/APTES sols and pure TEOS sols. In summary, four types of sols were electrospun, namely dye-doped sols further referred to as T/MR (TEOS/MR) sols, TA/MR (TEOS/APTES/MR) sols, and TA/MY (TEOS/APTES/MY) sols; and covalently bonded sols, further referred to as TA-MR (TEOS/MR-APTES) sols. T/MR membranes were produced according to the conditions in previous work, no influence of dye addition on electrospinning and the fiber properties was seen. This is in line with dye doping of polymer nanofibers, no influence of doping on the electrospinning process is seen.[16,27,29,30]

The optimum viscosity range for electrospinning of TA/MR, TA-MR, and TA/MY sols was in between 500 and 800 mPa s. In this viscosity range a stable electrospinning process was obtained and uniform, beadless nanofibrous membranes were produced. Scanning electron microscope (SEM) images of the membranes are shown in **Figure 3**. The reproducibility of these nanofibrous TA/MR, TA-MR, and TA/MY membranes was confirmed, with a similar average fiber diameter of 570 ± 140 nm, 585 ± 130 nm, and 674 ± 190 nm, respectively. Electrospinning of these sols was done for 2 h resulting in uniform, flexible, large (20 × 30 cm) nanofibrous membranes with a clear color.

The color of the TA/MR, TA-MR, and TA/MY samples was clearly different as shown in the inset of Figure 3. T/MR and TA/MR sols resulted in pink nanofibrous membranes while TA-MR and TA/MY sols resulted in orange nanofibrous membranes. This color difference can be attributed to the difference in pK_a of MR, MR-APTES, and MY, respectively 4.9 ± 0.2, 3.1 ± 0.1, and 3.3 ± 0.01. A pH of 3.6, 4.0, and 3.7 was measured for TA/MR, TA-MR, and TA/MY membranes, respectively, by first wetting with a drop of water followed by measuring the pH with a flat contact electrode. As a consequence, the MR in the TA/MR nanofibers is trapped in in its protonated forms (pH TA/MR membrane < pK_a MR). This results in the pink color of the membrane. MY and MR-APTES in the TA/MY and TA-MR nanofibrous membranes are trapped almost fully in their alkaline form (pH TA-MR and TA/MY membranes > pK_a

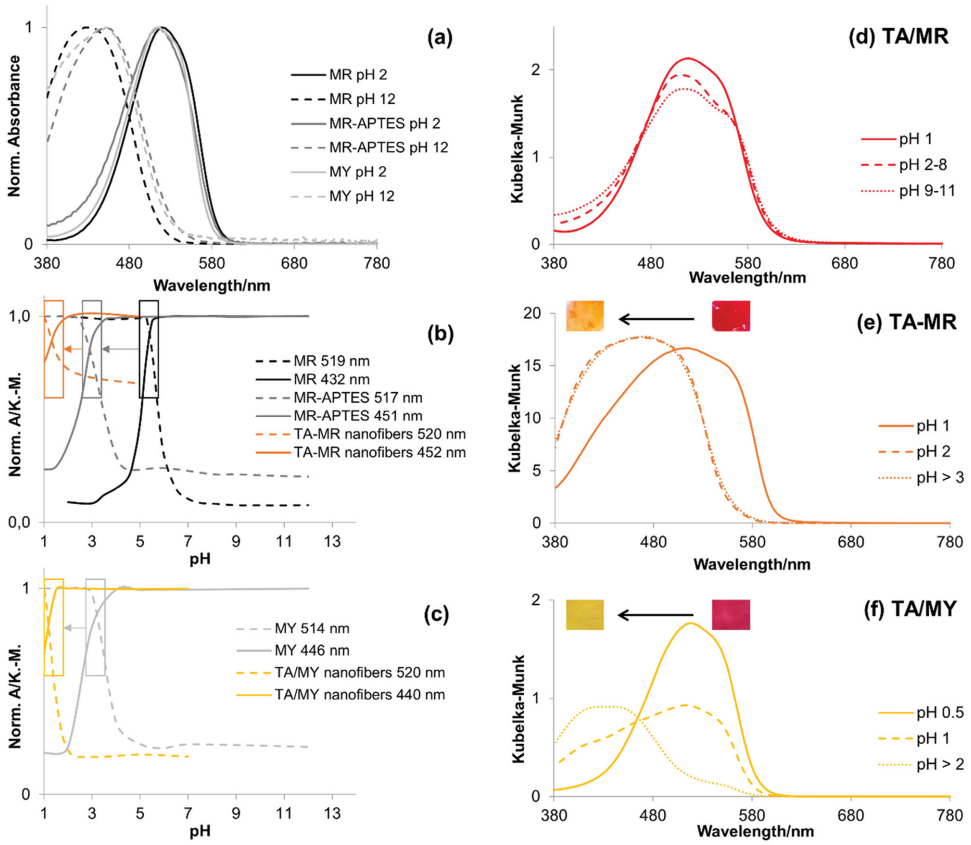

Figure 2. a) Normalized visible spectra of aqueous solutions of MR, MR-APTES, and MY illustrating their halochromic behavior. Visible reflection spectra of the nanofibrous structures illustrating the halochromic behavior of (e) covalently coupled TA-MR nanofibers, (f) dye-doped TA/MY nanofibers and illustrating the absence of halochromic behavior of (d) dye-doped TA/MR nanofibers. An overview of the pH-sensitivity window of the (b) MR, MR-APTES aqueous solutions and TA/MR nanofibers and (c) MY aqueous solution and TA/MY nanofibers is given, showing the clear shift in pK_a upon covalent linking of MR to APTES and the shift in pH-sensing range by incorporation into nanofibers.

MR-APTES and MY, respectively), which gives an orange color to the membrane.

2.4. Halochromic Behavior of Nanofibrous Membranes

The halochromic behavior of the nanofibrous membranes was tested both immediately after electrospinning and after storing for 21 d at high humidity (90% RH). During storing at high humidity, the samples became hydrophilic. This was confirmed via contact angle measurements. An average value of 136 ± 2° was found when a water droplet was placed onto the membranes before storing at high humidity. Afterward, a contact angle was no longer measurable (or thus 0°) and immediate wetting of the samples was seen. These changes in hydrophobic/hydrophilic behavior are attributed to surface water build up on the nanofibrous membranes in time, possibly combined with further crosslinking and/or the formation of silanol

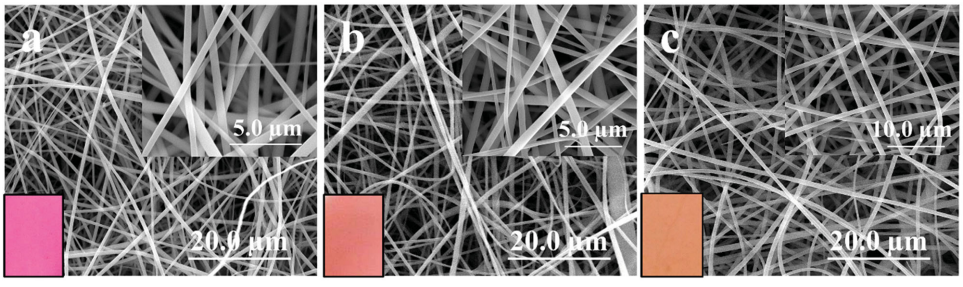

Figure 3. a) SEM images of TA/MR nanofibrous membrane, (b) SEM images of TA-MR nanofibrous membrane, and (c) SEM images of TA/MY nanofibrous membrane (color of the respective membranes is illustrated by pictures as inset).

groups by hydrolysis. This is confirmed via attenuated total reflectance Fourier-transform infrared (ATR-FTIR) where a peak broadening of the OH peak is seen (Figure S1, Supporting Information). It was confirmed that once the membranes become hydrophilic their properties are stable in time. The samples evaluated after storing at high humidity showed the same halochromic behavior as the samples before, but with a much faster response time. It is known that the wettability of the nanofibrous samples is a determining factor in the sensor response time.[29] This wettability is directly linked to the poor hydrophilicity of the as-spun nanofibers. Since the halochromic behavior is the same before and after storing, only the hydrophilic samples will be discussed in detail in the following.

The halochromic behavior of all samples is evaluated by immersing the samples in pH-baths from pH 1 till pH 12 (with a step of 1 pH-unit). The T/MR and TA/MR nanofibrous membranes did not show a color change, Figure 2d. This is attributed to the leaching of the dye from the silica matrix (Table S1, Supporting Information), which was expected since no chemical bond is formed between the dye and the silicon oxide network. Although the fabric did not change color as only the dye is retained that is not exposed to the aqueous environment, the leached dye did change color in the aqueous solution with the same halochromic behavior as the pure MR in aqueous solution.

The TA-MR nanofibrous membranes showed a more interesting halochromic behavior. A clear color change was seen from pink to orange, Figure 2e. After immersion of the TA-MR samples for 24 h almost no dye leaching (less than 2%) was seen and the samples remained deeply colored (Table S1, Supporting Information). Due to the hydrophilic behavior, these nanofibrous sensors revealed a response time within less than a second. The samples, which were orange at the start, changed to pink at pH 1. Increasing the pH above 2 resulted in the original orange color, with the color change being reversible. The acidic peak maximum and the alkaline peak maximum are found at 520 and 452 nm, respectively. Compared to MR-APTES in aqueous environment no peak shift was seen. However, a shift in pH-transition region to lower pH-values was noted compared to MR-APTES, for which a pK_a of 3.1 ± 0.1 was found (Figure 2b). A second shift of the pH-range is thus seen compared to MR-APTES in solution and pure MR in solution, Figure 2b. The change in transition pH can be attributed to the covalent bond formation of the MR-APTES with the silicon oxide matrix and the interaction of MR with the surrounding silicon matrix. This is in line with results on polymeric matrices where a shift in pK_a is seen when pH-indicator dyes are incorporated due to the dye-matrix interactions.[29,50] These TA-MR nanofibrous membranes can thus be used as acid sensor in aqueous environment. A movie visualizing the color change of the TA-MR membranes when immersing in water at pH 1 and pH 7 can be found in the Supporting Information.

The TA/MY nanofibrous membranes show a highly similar halochromic behavior as the TA-MR membranes (Figure 2f), however, dye leaching showed to be a major issue (Table S1, Supporting Information). The samples went from pink at pH 0.5 and pH 1 to yellow at pH 2 and higher. The acidic peak maximum at 520 nm shifts to the alkaline peak maximum at 440 nm, thus almost no difference in peak shift is noted compared to MY in solution. Nonetheless, a shift was seen in the pH-transition region to lower pH-values compared to MY in solution, for which a pK_a of 3.3 ± 0.01 was found (Figure 2c). This can again be attributed to the interaction of the dye with the surrounding silicon matrix. Due to the high dye leaching, 95% after 24 h immersion at pH 0.5, the TA/MY samples are not reusable as pH-sensor in aqueous environment. In comparison to TA/MR nanofibrous membranes, the dye leaching is slightly less for TA/MY and the halochromic behavior is slightly retained, which can be ascribed to the higher hydrophobicity of MY compared to MR leading to higher retention in the nanofibers.

In summary, the TA-MR membranes are highly suitable as pH-sensor in a strong acidic environment, where polymers are no longer usable. Moreover, a covalent bond between matrix and dye showed to be essential to obtain a fast, reversible, and reusable pH-sensor that can operate in aqueous environment.

2.5. HCl and NH_3 Gas Sensing

Sensing acid or alkaline atmospheres in an easy manner with a fast visual signal is highly valuable in industrial processes or in personal protective equipment and clothes. The color change of the TA/MR, TA-MR, and TA/MY nanofibers are evaluated and compared when they are exposed to HCl vapors and NH_3 vapors. T/MR nanofibers show a similar behavior as TA/MR and are not discussed in further detail. The samples were placed in a closed cuvette and the partial pressure of the tested gas was increased gradually. The TA/MR nanofibers, which were pink from the start, showed no color shift when exposed to HCl vapors (**Figure 4**a). However, a reduction of the peak width is measured with increasing partial pressure of HCl, which will lead to a brighter color. A difference in ΔE around 3 was measured, thus not clearly visual for the naked eye. The acidic peak maximum is slightly shifted from 504 to 508 nm upon exposure to HCl. As stated above, the TA/MR nanofibers have a pink color from the start and the MR is already trapped inside the nanofibers in its mono- and diprotonated forms. This is again confirmed with the HCl sensing by the absence of a color change. On the other hand, exposing the TA/MR nanofibers to NH_3 vapors resulted in an immediate visual color change of the fibers. They gradually change color from pink to yellow when the partial pressure of ammonia is gradually increased (Figure 4d). This is explained by the gradual deprotonation of the dye to the alkaline form, corresponding with a yellow color. The peak maximum shifts from 504 nm for the original sample to 456 nm when the sample is exposed to an excess of NH_3. The fast response time of seconds can be attributed to the typical characteristics of nanofibrous membranes: their high specific surface area and high porosity. When the samples are taken out of the cuvettes, they go back to their original color in around 20 min. This lag time provides a memory function that allows visual read-out up to 20 min after the exposure to NH_3 vapor, which is strongly desirable, for example, for personal protective equipment. These TA/MR membranes are thus ideal for sensing of NH_3 vapors.

HCl and NH_3 vapor sensing using the orange TA-MR and TA/MY nanofibrous membranes gives complementary results.

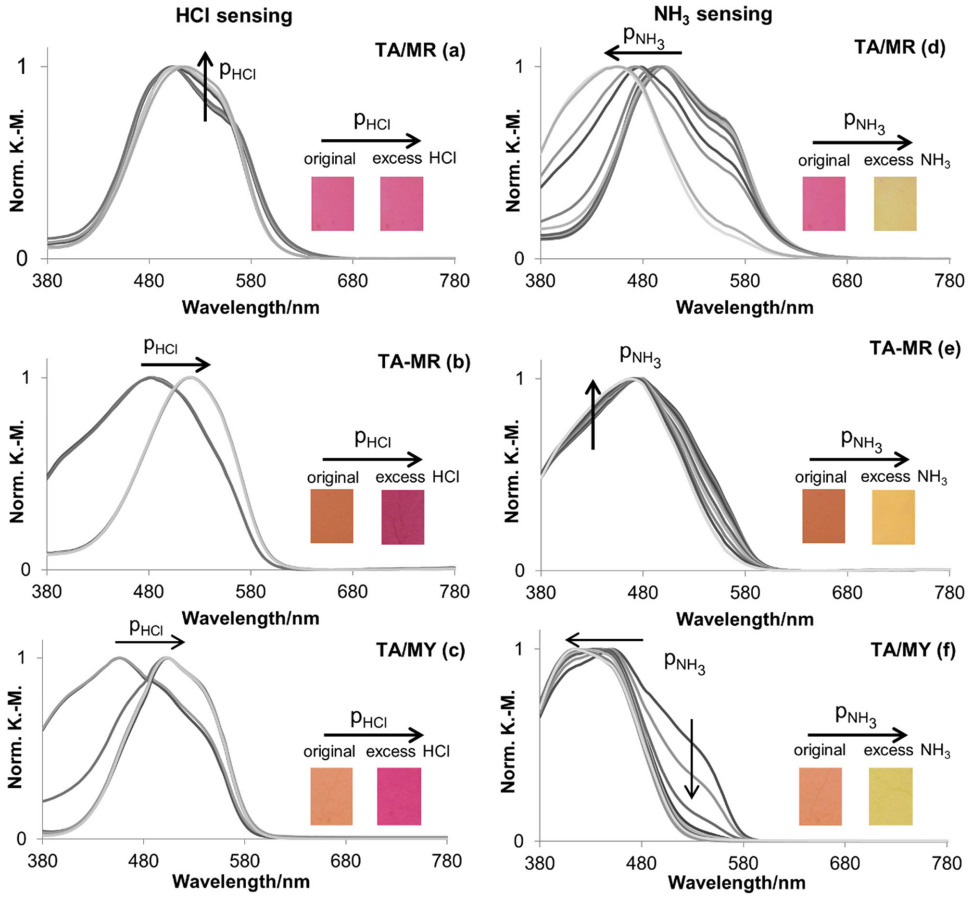

Figure 4. Normalized visible Kubelka–Munk spectra of TA/MR with increasing partial pressure of (a) HCl and (d) NH_3, Normalized visible Kubelka–Munk spectra of TA-MR with increasing partial pressure of (b) HCl and (e) NH_3, and normalized visible Kubelka–Munk spectra of TA/MY with increasing partial pressure of (c) HCl and (d) NH_3 (insets: pictures of sample showing the corresponding color transitions after exposure to vapors).

These nanofibers give a clear and immediate color change from orange to pink when exposed to HCl vapors (Figure 4b,c). The dye shifts from the alkaline to the protonated form. The peak maximum shows a bathochromic shift from 484 to 524 nm for TA-MR and from 456 to 504 nm for TA/MY upon exposure to HCl. The response to NH_3 vapors for these membranes is less clear. The color changes from orange to yellow (Figure 4e,f). This less-pronounced color shift, results from a peak narrowing for TA-MR and a peak shift from 452 to 416 nm for TA/MY. Again, the color change was immediate upon exposure to the vapors. A small amount of the dye seems to be present in the protonated form, shifting to the alkaline form upon exposure to NH_3, resulting in a color change from orange to yellow. A similar time period, around 20 min, was noted for the samples to go back to their original color after exposure to the vapors, again providing a valuable memory function. Complementary to the TA/MR nanofibrous, these TA-MR and TA/MY membranes are thus ideal for sensing of HCl vapors. In addition, they can be used for NH_3 sensing as well, although with a less clear visual response.

The sensitivity of the nanofibrous membranes was evaluated by gradually increasing the amount of HCl or NH_3 vapors to the closed cuvettes. **Figure 5** visualizes the color change ΔE as a function of partial pressure. HCl sensing was possible for TA-MR and TA/MY nanofibrous membranes with a visual color shift from orange to pink in between 160–300 ppm, and 100–300 ppm, respectively (partial pressure of 1×10^{-4} bar/5×10^{-5} bar – 2×10^{-4} bar, ΔE of 21 and 27, respectively), Figure 5 (left). For TA/MR there was no visual color shift with increasing partial pressure of HCl. NH_3 sensing was possible starting from 220 ppm or 2.85×10^{-4} bar (ΔE of 14) when using the TA/MR membranes, Figure 5 right. For these membranes the color shifted gradually, going from pink over orange to yellow. The excess amount of NH_3 resulted in a color difference ΔE of 40. A certain color can thus be linked with a certain partial pressure of NH_3 vapors. For the TA-MR and TA/MY nanofibrous membranes, a gradual shift from orange to yellow with gradual increasing partial pressure of NH_3 is seen. Although visually less clear to distinct, a yellow color started to appear at 220 ppm (2.85×10^{-4} bar). The color difference between the original sample and an excess of NH_3 is clearly visible (ΔE of 22 and 25, respectively), Figure 5 (right). A movie of the color change of TA-MR membranes upon exposure to excess amounts of HCl and NH_3 can be found in the Supporting Information.

Finally, the reversibility, reusability, and reproducibility is visualized in **Figure 6**. The TA/MR, TA-MR, and TA/MY

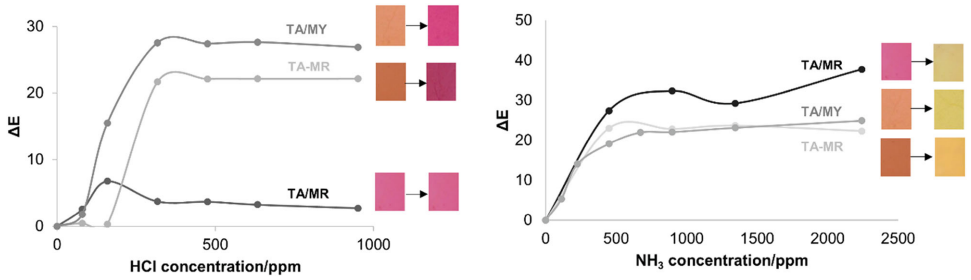

Figure 5. Color difference ΔE between original sample and sample exposed to HCl vapors as a function of HCl vapor concentration (left), color difference ΔE between original sample, and sample exposed to NH_3 vapors as a function of NH_3 vapor concentration (right) (insets: pictures of sample showing the corresponding color transitions after exposure to vapors).

samples were exposed to 10 cycles of HCl vapors alternated with NH_3 vapors. Each time an immediate color change was seen from pink to yellow or reversed. Thus confirming the reusability and stability of the colorimetric sensors.

2.6. Biogenic Amines Sensing

In addition to the sensing of ammonia and especially to demonstrate the versatility of the samples, the sensitivity of the samples for various biogenic amines that are released during decomposition of meat and fish was screened. The visual color change of TA/MR and TA-MR membranes were evaluated upon immersion in aqueous solutions of various biogenic amines with concentrations in the order of the limits that are allowed in food (**Table 1**).[51,52] The TA/MR nanofibrous samples showed a clear color change within less than a minute from pink to orange or yellow (Figure S2, Supporting Information), whereas the TA-MR gave a less visual but still noticeable color change from orange to yellow (Figure S3, Supporting Information). The results demonstrate that all tested amines except for tyramine resulted in clear visual color changes up to concentrations of 100 ppm and even 20 ppm for putrescine. In addition, TA/MR samples change color from pink to orange within 10 min above a 500 ppm trimethylamine (TMA) and dimethylamine (DMA) solution. Direct contact with the solution is thus not necessary, which offers the potential to use these membranes for food spoilage detection by incorporation in food packaging. These samples might thus, in addition to protective equipment, also be highly valuable for control and monitoring of food quality. Future work will focus on reduced dye leaching and covalent bonding of amine sensitive dyes on more compatible matrices for food applications.

3. Conclusion

Silicon oxide sols were functionalized with two halochromic dyes: methyl yellow and methyl red. The availability of a carboxylic acid group on MR gave the opportunity to covalently couple the dye to the sol-gel precursor APTES. MR was thus added via both doping and covalent bonding, MY on the other hand was only added to the silicon oxide sols via doping. All sols were electrospun via a stable reproducible electrospinning process, resulting in uniform, large, flexible, deeply colored nanofibrous membranes. The MR doped membranes were not

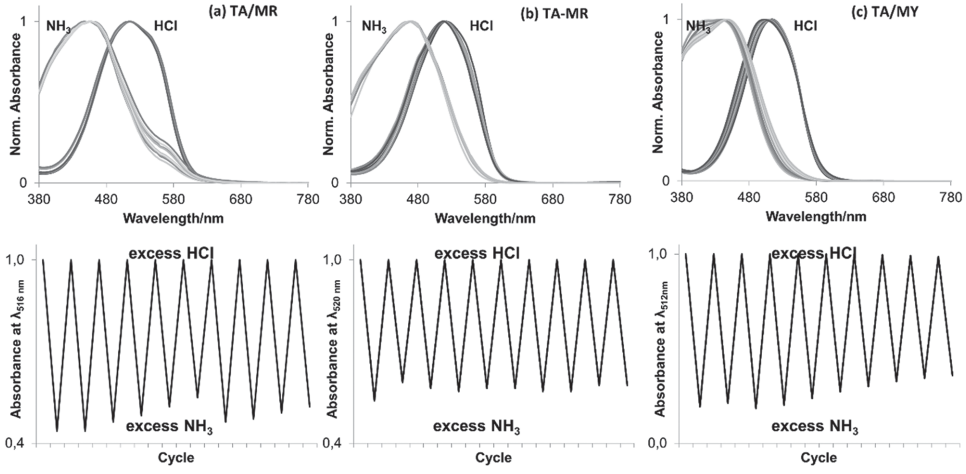

Figure 6. Reproducibility and reversibilty of HCl and NH_3 sensing with TA/MR, TA-MR, and TA/MY nanofibrous membranes: (top) normalised absorbance spectra of 10 cycles of excesses of HCl and NH_3; (bottom) absorbance at acidic peak maximum as a function of the cycle HCl or NH_3 of (a) TA/MR, (b) TA-MR, and (c) TA/MY.

Table 1. Color change of TA/MR and TA-MR membranes after immersion in biogenic amines solutions with various concentrations. +: Visual color change and – : no visual color change.

	TA/MR				TA-MR	
	5000 ppm	500 ppm	100 ppm	20 ppm	500 ppm	100 ppm
Histamine	+	+	+	–	+	+
Tyramine	–	–	–	–	–	–
Putrescine	+	+	+	+	+	+
Cadaverine	+	+	+	–	+	+
TMA	+	+	+	–	+	–
DMA	+	+	+	–	+	–

usable as pH-sensor in aqueous environment. The MY doped membranes and the MR covalently bond membranes showed a similar sensing behavior in aqueous environment. However, only the covalently coupled MR membranes were suitable to be used as pH-sensor in strong aqueous acidic environments, since dye leaching was a major problem for MY doped samples. A high sensitivity and fast response to HCl and NH_3 vapors was obtained for both MY doped and MR modified silicon oxide nanofibrous materials. MR doped samples were highly sensitive to NH_3 vapors. MY doped and MR covalently coupled membranes are sensitive for both HCl as NH_3 vapors. Large-area flexible sensors are developed that allow fast and accurate detection of local signals without the need of additional electronic devices. These nanofibrous membranes thus show to be ideal to be used as a visual warning patch in personal protective clothes or equipment since an immediate and clear color change is obtained upon exposure to hydrogen chloride or ammonia vapors. The more economical dye-doped membranes can thus be used for solid-state gas sensing applications where dye leaching is no issue, covalently functionalized membranes are however indispensable for applications where the sensors are exposed to liquids, e.g., rain. Finally, the sensitivity of these membranes to biogenic amines was demonstrated, showing their high versatility for multiple applications such as control of food quality.

4. Experimental Section

Materials: MY, MR, (3-aminopropyl)triethoxysilane (APTES, reagent grade 98%), dichloromethane (DCM, ≥99.8%), n-hexane (n-hex, 95%), and ethyl acetate (≥ 99.7%) were supplied by Sigma-Aldrich and used as received. Magnesium sulfate (dried) was supplied by Fisher Chemical. DCC was obtained from Sigma-Aldrich. DCC was purified by dissolving in DCM and drying using $MgSO_4$, yielding a pure wax solid after evaporation of the solvent. The sol-gel precursor TEOS (reagent grade 98%) was obtained from Sigma-Aldrich and used as received. The solvent absolute ethanol was obtained from Fiers. Hydrogen chloride (HCl, 37%) used as catalyst for the sols, used for the preparation of the pH-baths and used for the vapor experiments was also supplied by Sigma-Aldrich. Sodium hydroxide used for the preparation of the pH-baths and ammonium hydroxide solution (ACS reagent, 28–30% NH_3 basis) were also obtained from Sigma-Aldrich. Biogenic amines: DMA, TMA, and Histamine were obtained from Fluka. Putrescine and Cadaverine were obtained from Acros Organics and Tyramine was obtained from Sigma Aldrich. DMA and TMA were both solutions of 40 wt% in H_2O.

Functionalization of APTES with Methyl Red: Methyl red (MR, 0.510 g, 1.89 mmol, 1 eq) and DCC (0.494 g, 2.39 mmol, 1.26 eq) were dissolved in DCM (10 mL, anhydrous). This mixture was cooled to 0 °C after which APTES (0.44 mL, 1.88 mmol, 0.99 eq) was added dropwise. The temperature was allowed to heat up to room temperature while stirring. The reaction was followed using TLC (Silica, EtOAc/n-Hex 1/1, $R_{f,MR}$ = 0.2, $R_{f,MR\text{-}APTES}$ = 0.4) and appeared to be finished after 36 h after which the solvent was evaporated and the residual red sticky viscous solid was further purified using column chromatography yielding the product as a dark red solid. Yield: 0.321 g (36%), MS(ESI): m/z = 473.20 ($[M+H]^+$). ^{1}H NMR spectroscopy (300 MHz, DMSO-6d; Bruker Avance 300 MHz spectrometer): δ(ppm) 8.55 (t, J = 5.6 Hz, 1H, -C = O-*NH*-CH_2-), 7.85–7.39 (m, 6H, Ar H), 6.93–6.76 (m, 2H, Ar H), 3.82–3.62 (m, 6H, -O-*CH_2*-CH_3), 3.28 (t, overlaps H_2O, -NH-*CH_2*-CH_2-), 3.08 (s, 6H, -N-*$(CH_3)_2$*), 1.61 (dt, J = 12.6, 8.0 Hz, 2H, -CH_2-*CH_2*-CH_2-), 1.24–1.05 (m, 9H, -O-CH_2-*CH_3*), 0.71–0.50 (m, 2H, -CH_2-*CH_2*-Si-) (Figure S4, Supporting Information).

Fabrication and Characterization Methods: The dye-doped sols were prepared from a TEOS:APTES:MR(or MY):ethanol:water:HCl mixture with a molar ratio of respectively 1:0.0024:0.0024:2.2:2:0.01. First, TEOS was mixed with APTES, ethanol, and methyl red or methyl yellow in a beaker. Second, aqueous HCl was added dropwise to the mixture under vigorous stirring. After completion of the hydrolysis reaction, the sols were heated at 80 °C until the desired viscosity was reached. Finally, the sol was cooled down to room temperature. The same method was used for the sols for which MR was covalently bond to APTES. The molar ratio of TEOS:MR-APTES was again 1:0.0024. Also dye-doped sols without APTES were prepared with a similar TEOS:MR:ethanol:water:HCl molar ratio of 1:0.0024:2.2:2:0.01, respectively. Again the same preparation method was used.

Prior to electrospinning the viscosity of the sols was measured using a Brookfield viscometer LVDV-II. The electrospinning experiments were executed on a mononozzle set-up with a rotating drum collector. The tip-to-collector distance was fixed at 15 cm, the flow rate at 1 mL h^{-1} and the voltage was adjusted in between 20 and 24 kV to obtain a stable electrospinning process. All the experiments were executed at a relative humidity of 34% RH ± 5% of and a room temperature of 20 ± 1 °C. Nanofibrous membranes with a density of ±13 g m^{-2} were obtained.

The morphology and diameters of the nanofibers were analyzed using a scanning electron microscope (FEI Quanta 200F). Prior to SEM analysis, a gold coating was applied on the samples using a sputter coater (Balzers Union SKD030). The nanofiber diameters were determined via Cell D software. 50 measurements per sample were taken to calculate the average fiber diameters and standard deviations.

The contact angles of the nanofibrous membranes were characterized using a drop shape analyzer (DSA 30 KrÜss GmbH). Deionized water was used as solvent.

An ATR-FTIR spectrometer from Thermo Scientific was used to record spectra from 4000 to 400 cm^{-1} with a resolution of 4 cm^{-1}, 32 scans were taken for each experiment.

The UV–vis spectra were recorded using a Perkin-Elmer Lambda 900 spectrophotometer. 1 cm matched quartz cells were used for the transmission spectra of solutions and an integrated sphere (Spectralon Labsphere 150 mm) was used for the reflection measurements on the membranes. The spectra were recorded from 380 to 780 nm with a data interval of 1 nm for transmission and 4 nm for reflection. Absorbance values were used for transmission measurements. The reflection measurements were converted to Kubelka–Munk, Equation (1).

$$\frac{K}{S} = \frac{(1-R)^2}{2R} \quad (1)$$

The pH of aqueous solutions were measured with a combined reference and glass electrode (SympHony Meters VMR). Via a drop of demi water the pH of the direct environment of the nanofibrous membranes was measured using a flat pH-electrode (FlaTrode, Hamilton). The dye leaching was evaluated by immersing 5 mg of fabric in a water bath of 5 mL for 24 h. The dye migration was then determined by UV–vis spectroscopy. Both the normalized and nonnormalized UV–vis

spectra were used to evaluate the halochromic behavior. To visualize the halochromic color shift, the normalized absorbance and Kubelka—Munk spectra were plotted at the acidic and alkaline peak maximum as a function of pH. The vapor induced halochromic behavior of the samples was evaluated by placing a sample in a 1 cm matched quartz cell. The cell was closed using a septum and varying amounts of HCl and NH_3 vapors were inserted. The spectra were recorded in reflection. The vapor pressure of the vapors were determined via titration.

The color differences were determined out of the UV–vis spectra by CIE-Lab using D65/10° illuminant. ΔE was used to quantify the magnitude of the color differences using Equation (2), with ΔL, Δa, and Δb the differences in L, a, and b values, respectively. L represents the lightness, a and b are measures of redness/greenness and yellowness/blueness, respectively. More information on the calculation of color differences can be found in the Supporting Information (SI) of ref. [16]

$$\Delta E = \sqrt{\Delta L^2 + \Delta a^2 + \Delta b^2} \tag{2}$$

The pK_a values of MY, MR, and MR-APTES were calculated based on absorbance spectra using Equation (3). A_x is the absorbance obtained at a certain pH and A_a and A_b are the absorbance of the acid form and the base form of the dye, respectively.

$$pK_a = pH - \log\frac{A_x - A_a}{A_b - A_x} \tag{3}$$

Supporting Information

Supporting information is available from the Wiley Online Library or from the author.

Acknowledgements

J.G. and G.V. contributed equally to this work. The Agency for Innovation by Science and Technology (IWT) is gratefully acknowledged by J.G. and G.V. for funding the research through PhD grants. G.C. acknowledges the University of Leeds for the Rowe Goodall Bursary for her research stay at Ghent University.

Received: May 12, 2016
Published online: July 14, 2016

[1] O. Belhadj Miled, D. Grosso, C. Sanchez, J. Livage, *J. Phys. Chem. Solids* **2004**, *65*, 1751.
[2] C. Rottman, A. Turniansky, D. Avnir, *J. Sol-Gel Sci. Technol.* **1998**, *25*, 17.
[3] C. J. Brinker, G. W. Scherer, *Sol-Gel Science: The Physics and Chemistry of Sol-Gel Processing*, Academic Press, Inc., San Diego, CA, USA, **1990**.
[4] I. M. El-Nahhal, J. Livage, S. M. Zourab, F. S. Kodeh, A. Al swearky, *J. Sol-Gel Sci. Technol.* **2015**, *75*, 313.
[5] E. Wang, K.-F. Chow, V. Kwan, T. Chin, C. Wong, A. Bocarsly, *Anal. Chim. Acta* **2003**, *495*, 45.
[6] B. Gu, M. Yin, a. P. Zhang, J. Qian, S. He, *IEEE Sens. J.* **2012**, *12*, 1477.
[7] F. R. Zaggout, *Mater. Lett.* **2006**, *60*, 1026.
[8] F. R. Zaggout, N. M. El-Ashgar, S. M. Zourab, I. M. El-Nahhal, H. Motaweh, *Mater. Lett.* **2005**, *59*, 2928.
[9] S. Dong, M. Luo, G. Peng, W. Cheng, *Sens. Actuators B Chem.* **2008**, *129*, 94.
[10] E. Wang, K.-F. Chow, W. Wang, C. Wong, C. Yee, A. Persad, J. Mann, A. Bocarsly, *Anal. Chim. Acta* **2005**, *534*, 301.
[11] A. Persad, K.-F. Chow, W. Wang, E. Wang, A. Okafor, N. Jespersen, J. Mann, A. Bocarsly, *Sens. Actuators B Chem.* **2008**, *129*, 359.
[12] Y.-Y. Lv, J. Wu, Z.-K. Xu, *Sens. Actuators B Chem.* **2010**, *148*, 233.
[13] B. Ding, M. Wang, J. Yu, G. Sun, *Sensors* **2009**, *9*, 1609.
[14] L. Van Der Schueren, K. De Clerck, G. Brancatelli, G. Rosace, E. Van Damme, W. De Vos, *Sens. Actuators, B Chem.* **2012**, *162*, 27.
[15] L. van der Schueren, K. de Clerck, *Color. Technol.* **2012**, *128*, 82.
[16] I. Steyaert, G. Vancoillie, R. Hoogenboom, K. De Clerck, *Polym. Chem.* **2015**, *6*, 2685.
[17] L. Van Der Schueren, T. Mollet, Ö. Ceylan, K. De Clerck, *Eur. Polym. J.* **2010**, *46*, 2229.
[18] J. H. Wendorff, S. Agarwal, A. Greiner, *Electrospinning: Materials, Processing and Applications*, Wiley-VCH, Weinheim, Germany **2012**.
[19] S. Ramakrishna, K. Fujihara, W. E. Teo, T.-C. Lim, Z. Ma, *An Introduction to Electrospinning and Nanofibers*, World Scientific Publishing Co. Pte. Ltd, Singapore **2005**.
[20] S. Ramakrishna, K. Fujihara, W. E. Teo, T. Yong, Z. Ma, R. Ramaseshan, *Mater. Today* **2006**, *9*, 40.
[21] A. Greiner, J. H. Wendorff, *Angew. Chem. Int. Ed.* **2007**, *46*, 5670.
[22] D. Li, Y. Xia, *Adv. Mater.* **2004**, *16*, 1151.
[23] W. E. Teo, S. Ramakrishna, *Nanotechnology* **2006**, *17*, R89.
[24] L. Van Der Schueren, K. Hemelsoet, V. Van Speybroeck, K. De Clerck, *Dyes Pigm.* **2012**, *94*, 443.
[25] L. Van der Schueren, K. De Clerck, *Text. Res. J.* **2010**, *80*, 590.
[26] F. Di Benedetto, E. Mele, A. Camposeo, A. Athanassiou, R. Cingolani, D. Pisignano, *Adv. Mater.* **2008**, *20*, 314.
[27] A. Camposeo, F. Di Benedetto, R. Stabile, R. Cingolani, D. Pisignano, *Appl. Phys. Lett.* **2007**, *90*, 143115.
[28] A. Camposeo, L. Persano, D. Pisignano, *Macromol. Mater. Eng.* **2013**, *298*, 487.
[29] L. Van der Schueren, T. De Meyer, I. Steyaert, Ö. Ceylan, K. Hemelsoet, *Carbohydr. Polym.* **2013**, *91*, 284.
[30] A. Agarwal, A. Raheja, T. S. Natarajan, T. S. Chandra, *Sens. Actuators, B Chem.* **2012**, *161*, 1097.
[31] O. S. Wolfbeis, *Anal. Chem.* **2008**, *80*, 4269.
[32] S. Trupp, M. Alberti, T. Carofiglio, E. Lubian, H. Lehmann, R. Heuermann, E. Yacoub-George, K. Bock, G. J. Mohr, *Sens. Actuators, B Chem.* **2010**, *150*, 206.
[33] G. J. Mohr, H. Müller, B. Bussemer, A. Stark, T. Carofiglio, S. Trupp, R. Heuermann, T. Henkel, D. Escudero, L. González, *Anal. Bioanal. Chem.* **2008**, *392*, 1411.
[34] A. Lobnik, I. Oehme, I. Murkovic, O. S. Wolfbeis, *Anal. Chim. Acta* **1998**, *367*, 159.
[35] L. Van Der Schueren, K. De Clerck, G. Brancatelli, G. Rosace, E. Van Damme, W. De Vos, *Sens. Actuators, B Chem.* **2012**, *162*, 27.
[36] S. Tao, G. Li, J. Yin, *J. Mater. Chem.* **2007**, *17*, 2730.
[37] Y. Dai, W. Liu, E. Formo, Y. Sun, Y. Xia, *Polym. Adv. Technol.* **2011**, *22*, 326.
[38] D. Li, J. T. McCann, Y. Xia, M. Marquez, *J. Am. Ceram. Soc.* **2006**, *89*, 1861.
[39] R. Ramaseshan, S. Sundarrajan, R. Jose, S. Ramakrishna, *J. Appl. Phys.* **2007**, *102*, 1.
[40] G. Li, Z. Hou, C. Peng, W. Wang, Z. Cheng, C. Li, H. Lian, J. Lin, *Adv. Funct. Mater.* **2010**, *20*, 3446.
[41] P. Lu, B. Qiao, N. Lu, D. C. Hyun, J. Wang, M. J. Kim, J. Liu, Y. Xia, *Adv. Funct. Mater.* **2015**, *25*, 4153.
[42] J. Li, Y. Zhang, X. Zhong, K. Yang, J. Meng, X. Cao, *Nanotechnology* **2007**, *18*, 245606.
[43] S. Wen, L. Liu, L. Zhang, Q. Chen, L. Zhang, H. Fong, *Mater. Lett.* **2010**, *64*, 1517.
[44] J. Geltmeyer, L. Van der Schueren, F. Goethals, K. De Buysser, K. De Clerck, *J. Sol-Gel Sci. Technol.* **2013**, *67*, 188.

[45] J. Geltmeyer, J. De Roo, F. Van den Broeck, J. C. Martins, K. De Buysser, K. De Clerck, *J. Sol-Gel Sci. Technol.* **2016**, *77*, 453.
[46] Y. Yi, M. J. Farrow, E. Korblova, D. M. Walba, T. E. Furtak, *Langmuir* **2009**, *25*, 997.
[47] K. M. Tawarah, H. M. Abushamleh, *Dyes Pigm.* **1991**, *16*, 241.
[48] K. M. Tawarah, H. M. Abushamleh, *Dyes Pigm.* **1991**, *17*, 203.
[49] S. Bell, A. Bisset, T. J. Dines, *J. Raman Spectrosc.* **1998**, *29*, 447.
[50] T. De Meyer, I. Steyaert, K. Hemelsoet, R. Hoogenboom, V. Van Speybroeck, K. De Clerck, *Dyes Pigm.* **2016**, *124*, 249.
[51] *Public Health Risks of Histamine and Other Biogenic Amines from Fish and Fishery Products*, Meeting Report, FAO/WHO (Food and Agriculture Organization of the United Nations/World Health Organization) **2013**.
[52] A. Naila, S. Flint, G. Fletcher, P. Bremer, G. Meerdink, *J. Food Sci.* **2010**, *75*, R139.